Journal of Pharmaceutical Sciences xxx (2020) 1-10

Contents lists available at ScienceDirect

Journal of Pharmaceutical Sciences

journal homepage: www.jpharmsci.org

Pharmaceutics, Drug Delivery and Pharmaceutical Technology

Binder-Jet 3D Printing of Indomethacin-laden Pharmaceutical Dosage Forms

Shing-Yun Chang [a, b, 1], Si Wan Li [a, 1], Kavin Kowsari [a], Abhishek Shetty [c], Leila Sorrells [a], Koyel Sen [d], Karthik Nagapudi [e], Bodhisattwa Chaudhuri [a, d], Anson W.K. Ma [a, b, *]

[a] Department of Chemical and Biomolecular Engineering, University of Connecticut, Storrs, CT 06269, USA
[b] Polymer Program, Institute of Materials Science, University of Connecticut, Storrs, CT 06269, USA
[c] Anton Paar, 10215 Timber Ridge Drive, Ashland, VA 23005, USA
[d] Department of Pharmaceutical Sciences, University of Connecticut, Storrs, CT 06269, USA
[e] Genentech, Inc., 465 East Grand Avenue, South San Francisco, CA 94080, USA

ARTICLE INFO

Article history:
Received 8 April 2020
Revised 22 June 2020
Accepted 30 June 2020

Keywords:
3D printing
Inkjet printing
Binder jet
Ink rheology
Powder flowability

ABSTRACT

Emerging 3D printing technologies offer an exciting opportunity to create customized 3D objects additively from a digital design file. 3D printing may be further leveraged for personalized medicine, clinical trial, and controlled release applications. A wide variety of 3D printing methods exists, and many studies focus on extrusion-based 3D printing techniques that closely resemble hot melt extrusion. In this paper, we explore different pharmaceutical-grade feedstock materials for creating tablet-like dosage forms using a binder jet 3D printing method. In this method, pharmaceutical-grade powders are repeatedly spread onto a build plate, followed by inkjet printing a liquid binder to selectively bind the powders in a predetermined pattern. The physical properties of the pharmaceutical-grade powders and binders have been characterized and a molding method has been developed to select appropriate powder and binder materials for subsequent printing experiments. There was a correlation between the breaking forces of the molded and printed samples, but no clear correlation was observed for disintegration time, which was primarily controlled by the higher porosity of the printed samples. The breaking force and disintegration properties of as-printed and post-processed samples containing indomethacin as an active pharmaceutical ingredient have been measured and compared with relevant literature data.

Introduction

The need for individualized drug dosing as a function of patient's age, weight, and disease severity necessitates new drug delivery approaches. The recent approval of the U.S. Food and Drug Administration (FDA) of additively-manufactured (AM) drug tablets has triggered the emergence of pharmaceutical three-dimensional (3D) printing techniques.[1–4] Various suitable layer-by-layer 3D printing techniques exist for tablet fabrication, namely (i) stereolithographic (SLA),[5–7] which involves curing of photopolymers to produce 3D objects, (ii) binder-jet printing,[4,8–13] where an ink is patterned over a powder bed, (iii) selective laser sintering (SLS),[14–16] whereby a laser beam selectively-fuses portions of a powder bed, (iv) fused deposition modeling (FDM),[17–22] in which a thermoplastic filament is extruded through a high-temperature nozzle, (v) extrusion of a semi-solid through a nozzle,[23–26] and multi jet fusion (MJF), in which a fusing agent is printed onto a powder layer and energy is then applied to fuse the particles.[27–29] Among these techniques, binder jet printing provides a viable and a relatively simple manufacturing process of personalized drug dosing with the advantages of universal applicability, precise control of droplet size and volume, high reproducibility, and ability to produce complex drug-release profiles.[4,30–33] Compared to hot melt extrusion and laser-based powder bed fusion printing,[1,14,15,34] the near room temperature operation of inkjet-based binder-jet printing renders the process suitable for handling heat sensitive active pharmaceutical ingredients (API) and excipients.

* Corresponding author. Department of Chemical and Biomolecular Engineering, University of Connecticut, Storrs, CT 06269, USA.
E-mail address: anson.ma@uconn.edu (A.W.K. Ma).
[1] Equal contributions.

https://doi.org/10.1016/j.xphs.2020.06.027
0022-3549/

3D printing of pharmaceuticals, first pioneered in 1996, introduced digital control over the arrangement of drugs and excipients within a product.[35] The process involves distribution of thin layers of powder, selectively joined by dispensing droplets consisting of liquid binders. The unbound powder acts as support material for over-hung or hollow structures. API may either be jetted or included in the powder with additional excipients. Selection of appropriate ink-powder combinations provides opportunity for formulating a wide range of material combinations with potential use in a variety of drug delivery applications.[36–38] A number of process conditions determine the success of the binder jet method, including drop spacing, layer thickness, drop volume, binder fluid properties (e.g., viscosity and surface tension), and powder formulation.[39] The binder-jet 3D printing technique has been employed to achieve complex release profiles such as zero order (i.e., constant) release[40,41] and to create core-shell constructions.[10,41,42]

To date, a number of APIs have been successfully fabricated using the binder jet technique in conjunction with experimental investigations on the formulation of powder or binder excipients. Some examples include captopril, an angiotensin-converting enzyme inhibitor used to treat cases of hypersensitive emergency,[43] chlorpheniramine maleate,[44] pseudoephedrine hydrochloride (PEH),[41] and acetaminophen.[11] Recently, Infanger et al. (2018)[45] employed the powder bed method to print tablets containing caffeine as the model API. The authors concluded that tablet friability greatly depended on powder particle size, whereas disintegration time and dissolution properties depended largely on binder viscosity. Another recent study experimentally examined the effects of fifteen different excipients on microstructural appearance, friability, hardness, and disintegration time, whereby the observed trends may serve as a guide for efficient excipient formulation.[12] Despite the significant advances, material combinations for the binder-jet method are still rather limited. Commercial powders for rapid prototyping applications consist primarily of calcium sulfates or calcium carbonates,[46] and there is a need to explore new types of pharmaceutical excipient powder-binder combinations that can be effectively used in binder jet printing.

In this paper, we have studied a number of powders and liquid binders as possible feedstock materials for binder jet 3D printing of tablet-like solid dosage forms. Their physical properties have been characterized and benchmarked against standard feedstock materials provided by the printer manufacturer. A quick screening method has been developed to assess different powder-binder combinations and to select a powder type for further printing experiments with different binders. The attributes, namely, the breaking force and disintegration time, of various printed samples have been characterized and compared against existing literature data. Indomethacin, a nonsteroidal anti-inflammatory drug, has been used as a model drug to demonstrate the effectiveness of binder jet 3D printing as a process to make tablet-like dosage forms using common excipients.

Materials and Methods

Preparation of Feedstock Powders and Liquid Binders

Powders

VisiJet® PXL Core powder was supplied by the printer manufacturer (3D Systems) as their standard powder for rapid prototyping applications. VisiJet PXL Core powder contained 80–90% non-pharmaceutical grade calcium sulfate hemihydrate and 10–20% undisclosed ingredients. In this study, we evaluated a pharmaceutical-grade calcium sulfate hemihydrate (CSH; Fisher Chemical) and a pharmaceutical-grade lactose monohydrate (LM; Foremost) as the core base powders. In samples containing CSH, sodium croscarmellose (SC; Spectrum Chemical) was added as a disintegrant. In some formulations, Kollidon® VA64 (KL; BASF) was added as a binder to the print powder as a solid through v-blending. Indomethacin (Indo) powder was used as a model API (Letco Medical). All powders in the study were used as-received without further purification. Blending of powders, with and without the API, was carried out in a 16 L stainless steel V-blender (Patterson Kelley Blendmaster Twin Shell Liquid/Solids Blender). The weighted powders were loaded to the stainless-steel shell and blended at 25 rpm for 18 min at room temperature with a maximum volume loading of 40%.

Liquid Binders

Six different polymers were studied as a binding agent, including hydroxypropyl cellulose from Alfa Aesar (HPC), polyvinylpyrrolidone-vinyl acetate copolymer from BASF (Kollidon® VA64; KL), polyethylene glycol 3350 from Sigma-Aldrich (PEG), and three different hydroxypropyl methylcellulose products from Shin-Etsu (Pharmacoat 606; HPMC), Spectrum Chemical (HY122), and Dow Chemical (Methocel™ E5 Premium LV; MC). To prepare the aqueous binder solutions, the binder powders were fully dissolved in deionized water at room temperature, then passed through a 0.22 μm filter membrane using a vacuum filtration unit prior use. Filtering is important to reduce the chance of nozzle clogging.[47] The particle size distribution in the binder solutions was measured using light scattering before and after filtering. Light scattering experiments were carried out using an ALV compact goniometer system equipped with multi-detectors (CGS-3MD) (Germany), a 22-mW He–Ne laser (wavelength: 632.8 nm), and four avalanche photo diode detectors. Data are included in Supporting Information. The pH values of the binder in this study were measured at 25 °C using a pH meter (Fisher Accumet AB15). The pH values of the binders in this study range from 4.03 to 7.21, compared to the commercial VisiJet® clear liquid binder with a pH of 9.7 (See Supporting Information).

Binder Viscosity and Surface Tension Characterization

Viscosities of binder solutions were measured using a rheometer (Anton Paar MCR 702) equipped with a 40-mm parallel plate fixture for a shear rate ranging from 1 s^{-1}–200 s^{-1} at 25 °C. The surface tension values of the aqueous binder solutions were measured at 23 °C using a pendant drop tensiometer (DataPhysics OCA20) with a 1.8 mm-diameter needle and a dosing volume of 18 μl.

The Ohnesorge (Oh) Number and the Minimum Velocity Calculations

With the determination of the viscosity, density, and surface tension, the corresponding dimensionless viscosity, or the Ohnesorge (Oh) number, for the binders was calculated and shown in Fig. 2d. Oh is defined as:

$$Oh = \frac{\eta}{\sqrt{\gamma \rho d_n}} \tag{1}$$

where η is the viscosity, γ is the surface tension, ρ is the density, and d_n is the nozzle diameter (22 μm).[13] The value of Oh number, or the reciprocal of the Oh number ($Z = 1/Oh$), has been used as a predictor for the jettability of different viscous fluids based on their fluid properties.[48,49] Empirically, in the case of an Oh number larger than 1, inertia may not be sufficient to overcome the viscosity and surface tension, resulting in no jetting. Conversely, if the Oh number is smaller than 0.1, the ligament, or tail, of an ejected jet during

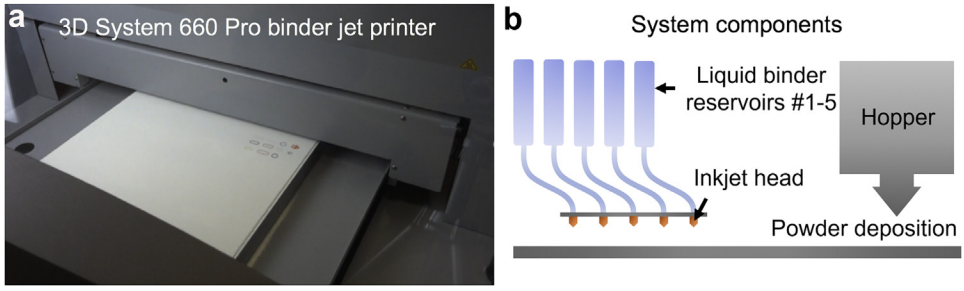

Fig. 1. Binder-jet 3D printing system for producing tablet-like dosage forms. (a) Photograph of the powder bed during printing. (b) Schematic of the system components.

printing may further break into finer droplets, termed "satellite drops", which are considered to be undesirable. Although the Reynolds (*Re*) and Weber (*We*) numbers cannot be directly calculated or measured in the current setup, a force balance between inertial and surface forces at the nozzle allows the estimation of the minimum drop velocity, which is given as[49]:

$$v_{min} = \sqrt{\frac{4\gamma}{\rho d_n}} \quad (2)$$

Powder Particle Size and Flowability Characterization

Particle size analyses were carried out using the Anton Paar Particle Size Analyzer PSA 1190 equipped with a dry dispersion unit. The PSA 1190 Particle Size Analyzer employs the laser diffraction technique to measure particles ranging from 0.04 to 2500 μm. The volume-based particle size distribution (PSD) has been recorded for the five powder samples (VisiJet® PXL Core, P1, P2, P3, and P4; see Table S1). An Anton Paar MCR-702 rheometer equipped with the powder cell accessory[50] and the Warren-Spring geometry (ST36-8V-10/PC/WS) was used to measure the Hausner Ratio (HR), Carr Index (CI),[51–53] and weighted Warren Springs cohesion strengths. Detailed data and discussions are included in Supporting Information.

Molding Experiments for Accelerated Formulation Screening

A mold containing 25 wells with a diameter of 8.4 mm and a depth of 5.3 mm was made by casting polydimethylsiloxane (PDMS; Silgard 184 Silicone Elastomer Kit) onto a 3D-printed inverse mold (Supporting Information). The inverse mold was printed using a Stratasys Connex350 3D printer and Digital ABS™ Ivory as the print material. The slurry was prepared by mixing 5 g of powder with 3 g of liquid. The liquid-to-powder ratio of 3:5 is chosen such that the mixture forms a slurry which can then be successfully molded into uniform and complete shapes for breaking force and disintegration testing. If the ratio is too low, the sample does not hold the shape when removed from the mold. Conversely, if the ratio is too high, the dried sample will deviate largely from the target size. Well mixed slurry was carefully poured to fill up each well. The excess portion was spread toward the sides with a razor blade. Slurry was then left to dry overnight in the mold and one day outside the mold before characterization. Each molded tablet weighs about 260 mg.

Binder-Jet 3D Printing Experiments

The 3D patterns of round- and oblong-shaped dosage forms with various dimensions were initially created in either CAD or STL file before being converted to ZBD file using the 3DPrint software (3D Systems). The tablet-like 3D printed dosage forms were created in a layered manner using a commercial binder-jet printer (660 CJP Pro, 3D Systems; Fig. 1a) that was modified with external reservoirs to reduce the amount of liquid binder required for printing. The printer is equipped with five HP 11 printheads based on bubble jet technology (Fig. 1b). The printing process was conducted at room temperature with the powder layer thickness of 100 μm using the 'vibrant' color setting to maximize the ink dose delivered to the powder. Upon the completion of a print job, the printed samples embedded in loose powder were first dried for 1.5 h at 40 °C and then left overnight at room temperature. Post-processing is adopted to enhance the breaking force of printed samples. Ten printed samples on an absorbent pad were placed under a nozzle of water sprayer at a distance of 10 cm. A total amount of ca. 4 mL of water was sprayed onto each side of as-printed samples, which were then left to dry overnight. In the binder jet printing experiments of this study, the active was introduced in the powder bed, and water was used as the ink. The total print time for the twelve tablets shown were about 30 min, excluding the drying time. The print time has not been optimized and can potentially be reduced by including more tablets laterally within the build envelope.

Characterization of Molded and 3D Printed Tablets

Breaking Force and Disintegration Test

The breaking force of molded and printed tablets was measured on a hardness tester (HT300 Tablet Hardness Tester, Key International), compliant with United States Pharmacopeia (USP) <1217> tablet breaking force protocol. Disintegration of the tablets was characterized on a tablet disintegration tester (Vanderkamp 10-911-71), which periodically submerges the test specimens at 30 cycles/min at 37.5 °C for 15 min, consistent with the USP <701> procedure. Reported breaking force and disintegration values were taken as averages of 6 tablets.

Determination of Indomethacin Content

Indomethacin content was determined using UV–Vis spectroscopy (Shimadzu UV-min) and expressed as the averaged weight percentage from three different tablets. Experimentally, the tablets were grounded, and 25–30 mg of the ground sample was mixed with ethanol (10 mL) and stirred for 2 h. After filtration with a 0.22-μm polytetrafluoroethylene (PTFE) filter and ten times dilution, the absorbance of solution at 319 nm was recorded. The calibration curve was generated by dissolving indomethacin in ethanol with a concentration ranging from 10 to 50 μg/mL.

Statistical Analysis

Statistical analysis was performed with the R statistical software. ANOVA was performed followed by a least significant difference (LSD) test to determine the statistical differences in the

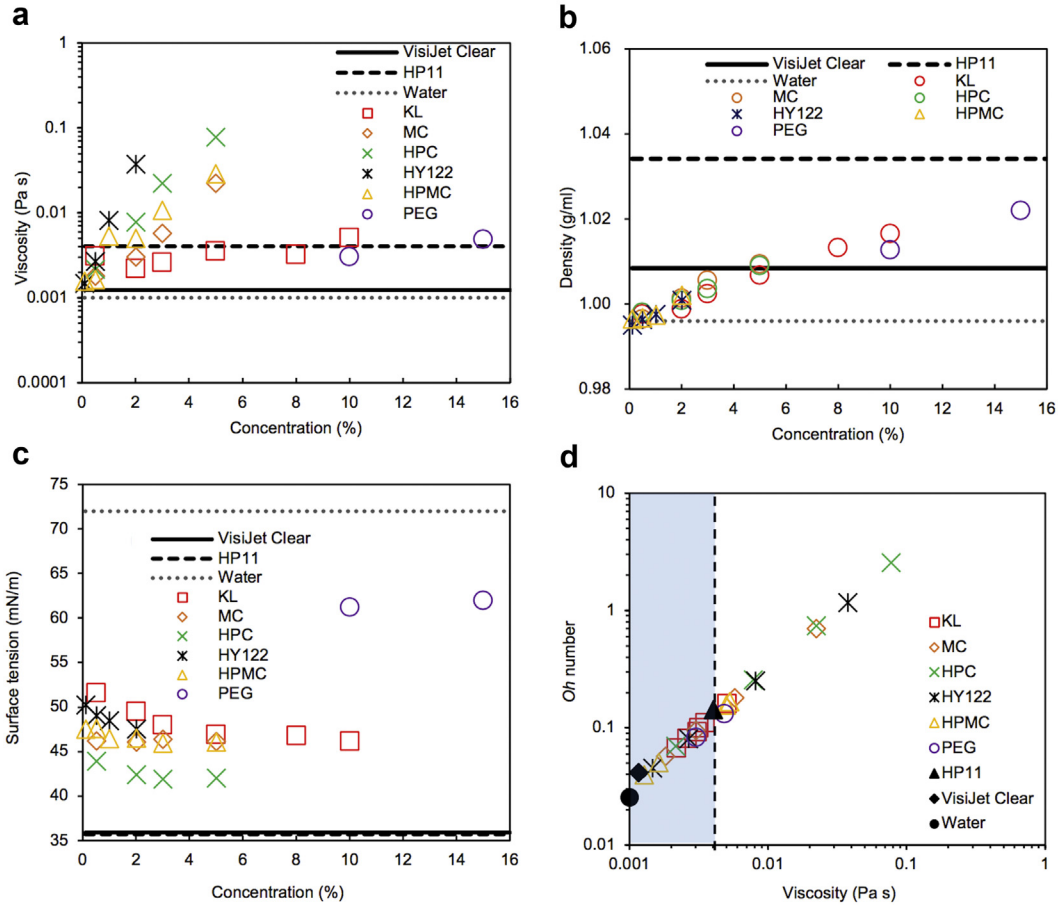

Fig. 2. Plots of: (a) apparent shear viscosity, (b) density, and (c) surface tension for various types and concentrations of binder solutions at 25 °C. (d) *Oh* number calculated for different binders using Equation (1).

group with a confidence interval of 95%. The statistical difference between two sets of data was determined by performing *t*-test.

Results and Discussion

Liquid Binder Properties and Selection

Fig. 2a–c shows the apparent shear viscosity, density, and surface tension data for the binders, an HP 11 black ink (Hewlett Packard), and VisiJet® PXL Clear (3D Systems). All test liquids behave like a Newtonian fluid for which the apparent shear viscosity is independent of shear rates. A shear rate of 10 s^{-1} was arbitrarily chosen for plotting the viscosity as a function of binder concentrations in Fig. 2a. As the binder concentration increases, both the shear viscosity and density increase, while the surface tension decreases. The decrease in surface tension may be explained by the presence of binder molecules at the interface due to excess Gibbs surface energy.[54] The higher the binder coverage or the surface activity of the binder, the lower the surface tension. As shown in Fig. 2c, the surface tensions of the custom binders were higher (42–52 mN/m) than those of the commercial inks (ca. 36 mN/m). The *Oh* number for the binders are shown in Fig. 2d. For binders with a shear viscosity less than that of the HP 11 ink, the *Oh* number ranges from 0.03 to 0.10, comparable to the that of the HP 11 ink and VisiJet® PXL Clear that have been specially formulated for the HP 11 print heads.

The minimum velocity is estimated to range between 2.83 m/s and 3.63 m/s for the binders selected in this study (Table 1), which is on par with a typical inkjet process.[55] Using the HP11 black ink as the benchmark, we further limit the binder concentrations such that the corresponding shear viscosity is below that of the HP11 ink in subsequent experiments. Table 1 summarizes the binders and selected concentrations, based on the highest concentration within the shaded zone in Fig. 2d, for subsequent molding and printing experiments.

Molding Experiments and Down Selection of Print Formulations for Scale Up

Many different combinations of powders and liquid binders are possible. Printing experiments require a considerable amount of powder (>15 kg) and binders (>1 L). Trial-and-error experiments are tedious and resource-intensive especially for experiments involving the use of API. Therefore, a quick screening method has been developed by molding the samples with different combinations of powders and liquid binders to understand the effect of each ingredient and their combinations on the breaking force and disintegration properties. This method, however, does not account for factors such as powder spreading and packing and the jettability and jetted volume of binders, which will also impact the properties of printed samples.

Effect of Different Liquid Binders

The effects of using different liquid binders on breaking force and disintegration for molded powder mixtures containing different levels of CSH are shown in Fig. 3a and b. For a given

Table 1
The Concentrations of Selected Liquid Binders, the Corresponding *Oh* Number and Estimated Minimum Drop Velocity.

Liquid Binder	Selected Concentration (w/w)	*Oh Number*	Estimated Minimum Velocity (m/s)
HPC	0.5%	0.07	2.83
HPMC	0.5%	0.05	2.95
HY122	0.1%	0.04	2.99
KL	8.0%	0.10	2.90
MC	0.5%	0.06	2.90
PEG	10%	0.08	3.32
Water	N/A	0.03	3.63

powder composition, Kollidon® VA64 (KL) consistently produced samples with a higher breaking force, compared to other liquid binders, including MC, HPC, HY122, HPMC, PEG, and water (Fig. 3a). It should, however, be noted that the binder concentration varies from binder to binder and is chosen to be the highest possible concentration for keeping the viscosity lower than the benchmark HP 11 ink (see Fig. 2d). Except in the case of KL, the breaking force increases as the CSH content increases progressively from 0% to 40%. Interestingly, the breaking force of molded samples prepared from 100% LM (with 0% CSH) shows the second highest breaking force that is below that of 40% CSH, but higher than that of 30% CSH. We hypothesize that KL interacts with the dissolved LM and reduced the crystallinity of LM upon drying, which consequently increased the bonding capacity and breaking force, consistent with previous studies.[56–58] In terms of disintegration, the 100% LM samples fully disintegrated in less than 7 min as shown in Fig. 3b. For subsequent printing experiments, we have chosen LM as the filler for achieving fast disintegrating formulations.

Effects of KL Concentration and Method of Introduction

In binder jetting, KL may be added in two different ways, namely, (i) as a solid to the feedstock powder while using pure water as the liquid binder, or (ii) is first dissolved in water and then printed onto the powder as a liquid. The results from molding experiments (Fig. 3c) showed that the method of KL introduction has no noticeable effect on the breaking force and disintegration time provided that the same amount of KL is used. However, as mentioned before, molding experiments do not account for the ink jettability and jetted volume during actual printing. Introducing KL in the solid form for binder jetting will likely allow a higher amount of KL be introduced to the sample as the KL loading in the printed samples will not be limited by factors like the viscosity and

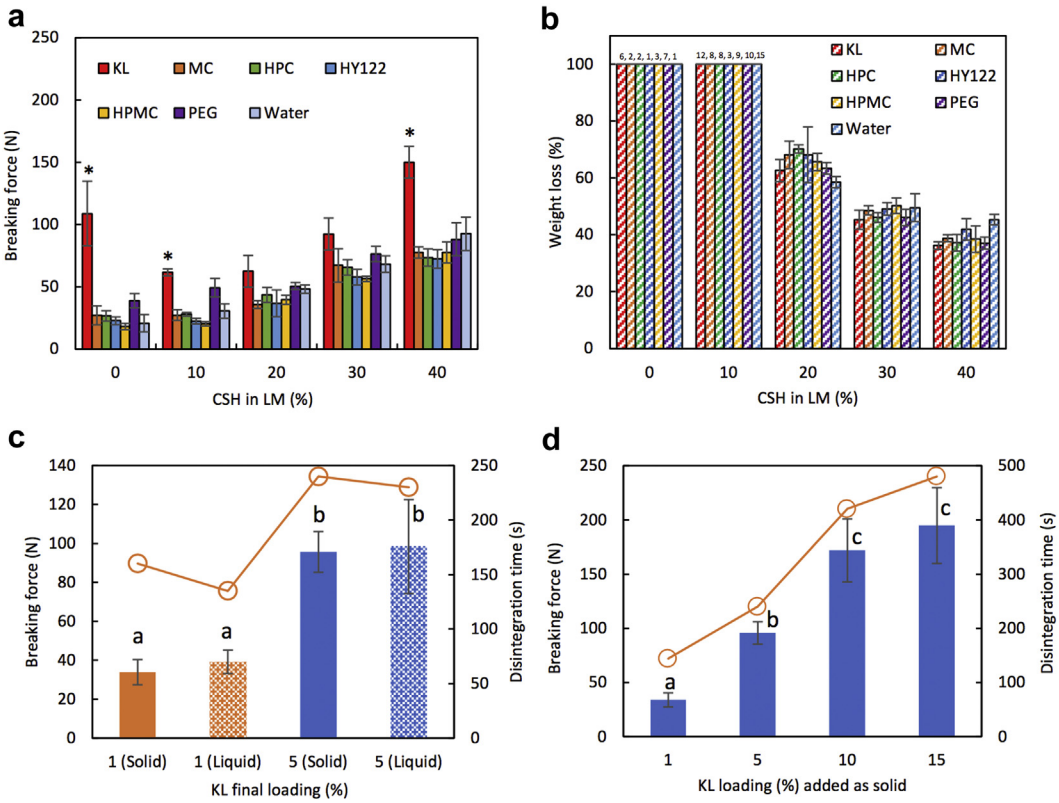

Fig. 3. (a) Breaking force and (b) disintegration data of molded tablets for different binders (Table 1) and powder mixtures containing different amounts of CSH. For fully disintegrated samples, the number above the bar indicates the corresponding disintegration time in minutes. "*" denotes significant difference at $p < 0.05$ according to the LSD test. The error bar represents the standard deviation from measuring six samples. (c) Breaking force and disintegration data for different methods of KL introduction, in which a fixed amount of KL is introduced either as a solid powder or in the form of an aqueous solution. (d) shows the effect of KL loading on breaking force and disintegration times of molded samples when KL is added as a solid. Same letter denotes the data are insignificantly different, based on a one-way ANOVA and LSD test ($p < 0.05$).

jettability of the aqueous KL solutions. Further, introducing KL in the powder form will also prolong the longevity of the bubble jet print head, in which the heater is more susceptible to fouling and a low pH if KL is introduced in the liquid form. The pH of an aqueous 8% KL solution was measured to be 4.03. For these reasons, printing experiments focus on using KL in the powder form by first blending it with the excipient and/or API while pure water is used as the liquid binder. Having decided on the method of KL introduction, the effects of KL concentration on the breaking force and disintegration are shown in Fig. 3d. As the KL loading increases, both the breaking force and disintegration time increase. Increasing the KL loading from 5% to 10% increases the breaking force by about 80% whereas further increasing from 10% to 15% only moderately increase the breaking force by an additional 13%. Based on these results, 10% KL was introduced in the powder form in the subsequent binder jetting experiments.

LM-KL vs. LM-CSH Powder Mixtures and Introduction of Disintegrant (SC)

An Ashby plot[59] was generated based on the data shown in Fig. 3, showing the breaking force and disintegration times for LM samples blended with different levels of KL and CSH powder (Fig. 4). There are a few outliers, but several trends can be observed. First, in line with expectations, as the breaking force increases, disintegration time also increases. Second, LM-KL powder mixtures tend to produce molded samples with a higher breaking force compared to LM-CSH powder mixtures. This is consistent with the previous explanation that KL interacts with the dissolved LM and increase the bonding force upon drying. Third, compared to LM-KL samples, the breaking force of the samples molded from a LM-CSH powder mixture is rather insensitive to the mixing ratios and the choice of binder (except when KL is used as the liquid binder). The detailed results are tabulated in Supporting Information. There appears to be two distinct operating lines depending on whether CSH is added or not. In the case of powder mixtures that contained 20% or more CSH, they did not fully disintegrate within 900 s.

Sodium croscarmellose (SC), was added as a disintegrant to the powder mixtures of CSH and LM, to promote disintegration. The effects of adding 5% SC (by weight) to mixtures containing different levels of CSH was shown in Fig. 5a and b. SC increased the weight loss in disintegration experiments by about 37%, 36%, and 7% for 20%, 30% and 50% CSH in LM, respectively. Inclusion of SC also affected the breaking force. 5% SC increased the breaking force for 20% CSH by 59% and had no impact on the breaking force of molded samples containing 30% CSH. However, adding 5% SC to 1:1 mixture of CSH and LM (i.e., 50% CSH in LM) significantly reduced the breaking force by 57%. Based on these observations, it was decided to use 100% LM as a filler for at scale binder jet 3D printing experiments.

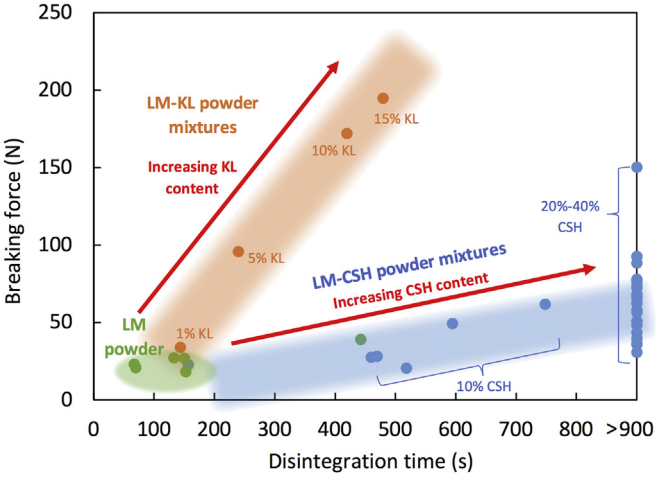

Fig. 4. Breaking forces and disintegration times of molded samples prepared from 100% LM powder (green), LM-KL (orange) and LM-CSH powder mixtures (blue). The shades are added to guide the eyes. The exact formulations and corresponding breaking force and disintegration data are included in Supporting Information. Samples containing 20%–40% CSH did not fully disintegrate within 900 s (15 min).

Binder Jet 3D Printing Experiments

Correlation Between Printed and Molded Samples

The molding test was developed as a material-sparing method to quickly understand the formulation compositions that would provide adequate breaking force and disintegration times. It is not expected that properties of the molded tablets would quantitatively translate to tablets made by binder jet printing. However, the properties are expected to correlate between the two methods. We have plotted the breaking force and disintegration time of the molded and printed samples (Fig. 6). There is a good correlation between the breaking force of the molded versus printed samples. There is, however, no strong correlation between the disintegration times of the molded versus printed samples. All the printed samples showed rapid disintegration compared to the molded counterparts. The fast disintegration of the printed samples is attributed to their higher porosity compared to the molded samples. Based on the measured bulk density (ρ_b) and LM particle density (ρ_p) of 1.55 g/cm^3,[60] the porosity of the printed samples ($\varphi = 1 - \rho_b/\rho_p$) is estimated to vary from 0.50 to 0.61, whereas that of the molded samples varies from 0.33 to 0.49 (see Supporting Information). Thus, molding test can be used as a surrogate for tablet breaking force but not for disintegration time.

Shape Control and Variation

Tablets with two different shapes, namely, round and oblong (Fig. 7), were printed using 100% LM as the filler and different liquid binders to: (i) demonstrate the versatility in changing the shape of the tablets and (ii) quantitatively assess the variation in size and weight from tablet to tablet. First, in the case of a round tablet design, a diameter of 8.2 mm and a thickness of 5.3 mm were arbitrarily chosen. The average diameter of the tablets printed with different binders varies from 8.2 mm (for 0.1% HY122) to 9 mm (0.5% HPMC) while the thickness varies from 5.1 mm (for 8% KL) to 6.2 mm (for 0.5% MC). The diameter and thickness deviate from those in the design file by less than 10% and 17%, respectively. For oblong tablets, a length (long axis) of 15.6 mm, a width (short axis) of 7 mm, and a thickness of 5.3 mm were specified in the digital design file. The printed tablets have an average length ranging from 15.3 mm (for 0.1% HY122 and water) to 15.9 mm (for 0.5% HPMC), an average width from 7.3 mm (for 0.5% HPC) to 8 mm (0.5% HPMC and 10% PEG), and an average thickness from 4.9 mm (for 0.5% HPC) to 6.5 mm (for 10% PEG). The deviations for length, width, and thickness are less than 2%, 14%, and 23%, respectively. The deviations may be explained by the lateral spreading and penetration depth as a given binder is deposited onto the powder bed. In terms of tablet-to-tablet variation, the deviation is small, less than 10% for physical dimensions and 2% for the weight, regardless of the shape. Detailed results are tabulated in Supporting Information. As shown in Fig. 7a and b, the use of 8% KL as a liquid binder produced samples with a noticeably larger breaking force independent of the shape, similar to the molding test results.

Some difference in breaking forces was observed between the round and oblong printed samples, especially for 0.5% HPMC and 0.5% MC (Fig. 7a and b). The stress distribution within a tablet loaded under diametrical compression is rather complex. The

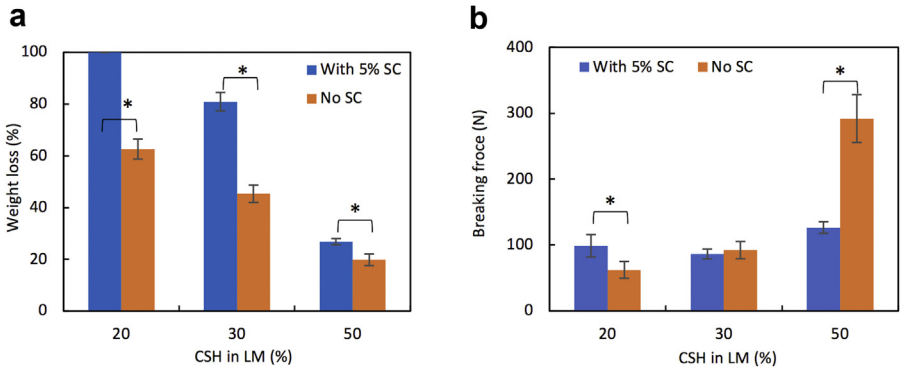

Fig. 5. (a) Weight losses in disintegration experiments and (b) breaking forces with and without 5% SC added for 20%, 30% and 50% of CSH in LM. "*" denotes a statistically significant difference between with and without SC based on *t*-test ($p < 0.05$).

breaking force depends on the exact shape of the sample, materials, and other factors such as the internal density distribution, loading conditions, and failure criteria.[61,62] The effect of tablet shapes on the measured mechanical properties has been reported and remained an active research area.[62,63] In this study, the tensile strengths of the round and oblong samples were calculated from the breaking forces and the actual dimensions of the tablets using the equations proposed by Pitt and Heasley.[63] For a given binder, *t*-test has been performed to compare the calculated tensile strengths of round versus oblong tablets. The results are included in Supporting Information. The tensile strengths of the oblong printed samples are consistently lower than those of the corresponding round printed samples, in agreement with the theoretical predictions based on finite element analysis (FEA).[63]

Printing With Active and Dose Variation

Using optimized parameters obtained from the placebo experiments, printing round tablets with Indomethacin (Indo) as the model API was attempted. 10% KL and 5% Indo were added to the LM filler and water was used as the binder. The resultant tablets have a breaking force of 28.4 ± 2.9 N and a disintegration time of 5 s. By spraying a fixed amount of water in a post-processing step (see Materials and Methods), the breaking force of the as-printed increased to 77.4 ± 3.9 N while the disintegration time increased to 30 s. However, these values are still lower compared to the molded tablets with the same composition, possibly because of the limited liquid binder amount and/or the exact powder packing during 3D printing. Attempts to measure the amount of jetted liquid binder directly by weighing the reservoir before and after printing were unsuccessful as the turnkey printer was programmed to purge the print nozzles using the binder solutions. However, the total amount of liquid binder used for printing and purging, was estimated to be 449 and 168 mg/tablet for water and 8% KL, respectively, suggesting a much less amount of ink was jetted with KL inclusion. In a separate study, it was estimated that the jetted binder volume varied from 5 mg to 45 mg (per tablet) by jetting a liquid binder containing the drug and measuring the final drug content in the printed samples using an assay. Fig. 7c shows the cross-sections of a molded, as-printed, and post-processed tablet. The post-processed sample has densified showing a smaller volume after exposure to water and drying. The active (indomethacin) content in the powder bed, as-printed tablets, post-processed tablets, and molded tablet were measured by UV−vis spectroscopy. As shown in Fig. 7d, the content in the as-printed and post-processed tablets are comparable to that in the powder bed (prior to printing) and molded samples. No significant degradation has been observed after printing and post-processing. Fig. 8 compares the breaking force and disintegration time of the printed tablets in this study (filled symbols) with those reported in the literature for LM and sucrose-based powders (unfilled symbols). First, all the LM-based printed samples in this study have a disintegration time less than 30 s. As disintegration time of the printed tablets is fast, complete release of drug is expected to occur rapidly. As a result, quantitative drug release studies were not pursued owing to the immediate release nature of the samples. Second, the breaking force values of the as-printed samples in this study are comparable to that reported in[10] and[12] but lower than that in,[13] which uses LM as base powder and 4-

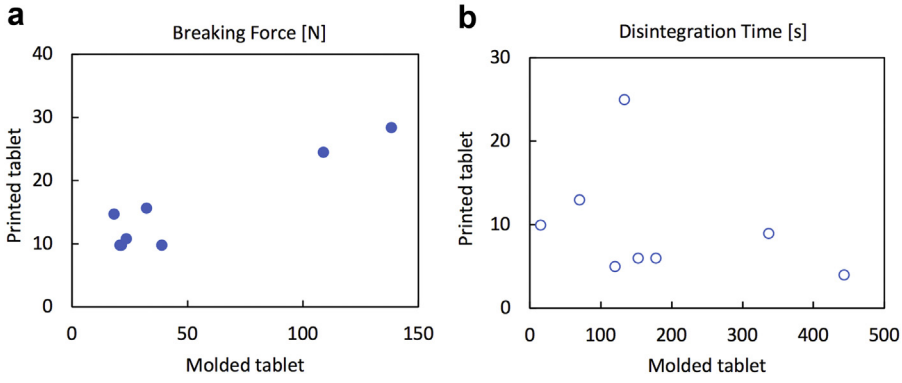

Fig. 6. (a) Breaking forces (N) and (b) disintegration times (s) of printed versus molded samples.

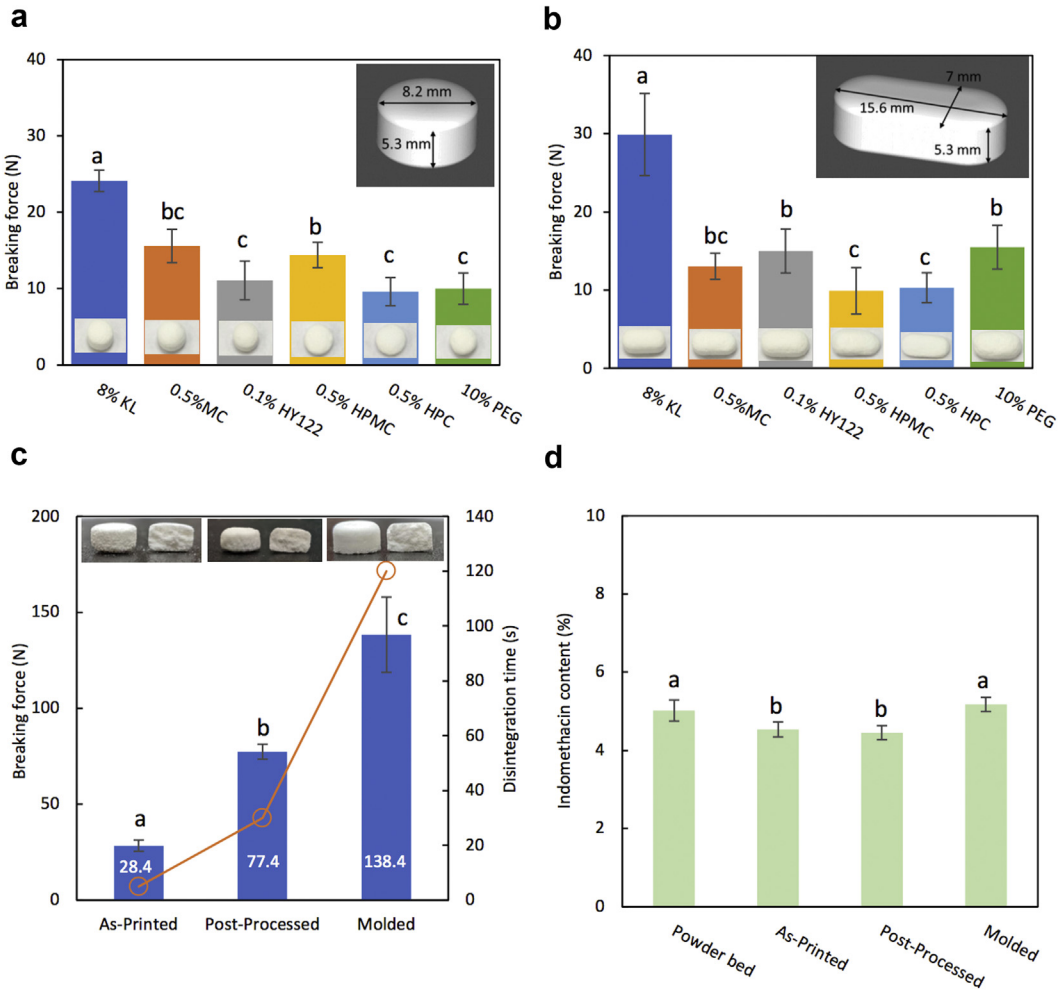

Fig. 7. Breaking forces of (a) round and (b) oblong samples printed with 100% LM and different binders. Inset figures (in the top right corner) show the input CAD design models and dimensions. (c) Breaking forces (bars) and disintegration times (circles) of as-printed, post-processed and molded samples containing 85% LM, 10% KL, and 5% Indo. (d) Indomethacin contents in the powder bed, as-printed, post-processed and molded samples. Same letter denotes the data are insignificantly different at $p < 0.05$ according to the one-way ANOVA and LSD test.

arm star poly(vinyl pyrrolidone) as binder. With post-processing, the breaking force of the printed sample containing active surpassed that reported in.[13]

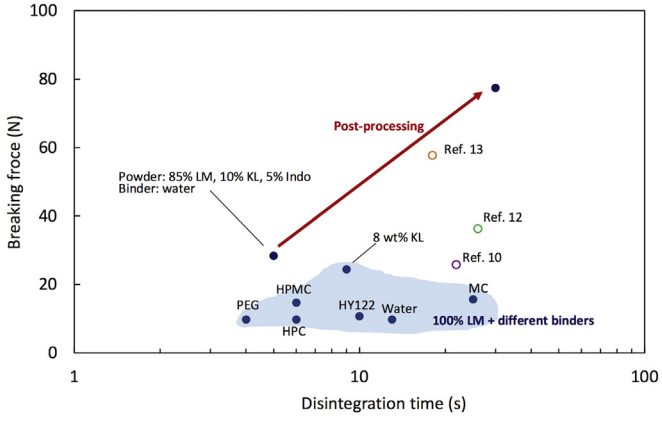

Fig. 8. Breaking forces and disintegration times of 3D printed samples. Filled symbols: this work. Unfilled symbols are literature data for sucrose[12] and lactose-based 3D printed tablets.[10,13]

Conclusions

A number of pharmaceutical-grade powders and liquid binders were characterized and evaluated as feedstock materials for an inkjet-based 3D printing method called “binder jet”, in which the powders are spread and bound by a liquid binder in a layer by layer manner to create 3D objects from a digital design file. A molding method has been developed and employed to accelerate the screening of different powder and binder combinations. This material-sparing method further allowed the selection of a powder type for further 3D printing experiments. A commercially available binder jet 3D printer has been adapted for successfully printing of tablet-like dosage forms using different binders. The appropriate binder concentrations were determined based on benchmarking the fluid properties of the custom binders against a commercial ink for the specific print head used in this study. Kollidon® VA64 (KL) consistently produced molded and printed tablets with a higher breaking force. The KL binder may be added as a powder to the print powder or in the form a liquid binder after dissolving KL in water. There is no statistical difference in terms of the breaking force values of the molded samples given that the same amount of KL is used. However, the powder route is preferred in 3D printing to circumvent the limitations in jetting a higher viscosity liquid with a

bubble jet print head. The breaking force and disintegration properties of the samples printed with different binders were characterized and compared against literature data. There is a correlation between the breaking forces of the molded and printed samples, but no clear correlation between the disintegration times of the two is observed. Disintegration times of the printed samples are considerably shorter than the molded counterparts, probably because of the higher porosity of the printed samples. The breaking force of as-printed samples is limited by the amount of binder jetted using the bubble jet print heads, but the results are comparable to those previously reported. A post-processing method, which involves spraying water onto the as-printed sample, increases the breaking force while maintaining the desired disintegration time. The ability of this technique to manufacture tablets using Indomethacin as a model API at a loading of 5% was also demonstrated. The content of Indomethacin in the as-printed and post-processed samples closely match those in the print powder and molded samples.

Acknowledgements

The authors would like to acknowledge financial support from Genentech (USA), Joseph Luciani for 3D printing the inverse mold, BASF Pharma Solutions (USA) and Kerry Inc. (USA) for providing in-kind materials for evaluation, and Anton Paar USA for instrument support.

Appendix A. Supplementary Data

Supplementary data to this article can be found online at https://doi.org/10.1016/j.xphs.2020.06.027.

References

1. Norman J, Madurawe RD, Moore CM, Khan MA, Khairuzzaman A. A new chapter in pharmaceutical manufacturing: 3D-printed drug products. *Adv Drug Deliv Rev*. 2017;108:39-50.
2. *Administration, U. S. F. a. D., Highlights of Prescribing Information—Spritam*. 2015.
3. Awad A, Trenfield SJ, Goyanes A, Gaisford S, Basit AW. Reshaping drug development using 3D printing. *Drug Discov Today*. 2018;23(8):1547-1555.
4. Trenfield SJ, Madla CM, Basit AW, Gaisford S. Binder jet printing in pharmaceutical manufacturing. In: *3D Printing of Pharmaceuticals*. Springer; 2018:41-54.
5. Wang J, Goyanes A, Gaisford S, Basit AW. Stereolithographic (SLA) 3D printing of oral modified-release dosage forms. *Int J Pharm*. 2016;503(1-2):207-212.
6. Martinez PR, Goyanes A, Basit AW, Gaisford S. Influence of geometry on the drug release profiles of stereolithographic (SLA) 3D-printed tablets. *AAPS PharmSciTech*. 2018;19(8):3355-3361.
7. Martinez PR, Goyanes A, Basit AW, Gaisford S. Fabrication of drug-loaded hydrogels with stereolithographic 3D printing. *Int J Pharm*. 2017;532(1):313-317.
8. Prasad LK, Smyth H. 3D Printing technologies for drug delivery: a review. *Drug Dev Ind Pharm*. 2016;42(7):1019-1031.
9. Kyobula M, Adedeji A, Alexander MR, et al. 3D inkjet printing of tablets exploiting bespoke complex geometries for controlled and tuneable drug release. *J Control Release*. 2017;261:207-215.
10. Yu D-G, Branford-White C, Yang Y-C, Zhu L-M, Welbeck EW, Yang X-L. A novel fast disintegrating tablet fabricated by three-dimensional printing. *Drug Dev Ind Pharm*. 2009;35(12):1530-1536.
11. Yu DG, Yang XL, Huang WD, Liu J, Wang YG, Xu H. Tablets with material gradients fabricated by three-dimensional printing. *J Pharm Sci*. 2007;96(9):2446-2456.
12. Tian P, Yang F, Yu L-P, et al. Applications of excipients in the field of 3D printed pharmaceuticals. *Drug Dev Ind Pharm*. 2019;45:905-913.
13. Wilts EM, Ma D, Bai Y, Williams CB, Long TE. Comparison of linear and 4-arm star poly (vinyl pyrrolidone) for aqueous binder jetting additive manufacturing of personalized dosage tablets. *ACS Appl Mater Interfaces*. 2019;11(27):23938-23947.
14. Fina F, Goyanes A, Gaisford S, Basit AW. Selective laser sintering (SLS) 3D printing of medicines. *Int J Pharm*. 2017;529(1-2):285-293.
15. Fina F, Goyanes A, Madla CM, et al. 3D printing of drug-loaded gyroid lattices using selective laser sintering. *Int J Pharm*. 2018;547(1-2):44-52.
16. Sadia M, Alhnan MA, Ahmed W, Jackson MJ. 3D printing of pharmaceuticals. In: *Micro and Nanomanufacturing Volume II*. Springer; 2018:467-498.
17. Water JJ, Bohr A, Boetker J, et al. Three-dimensional printing of drug-eluting implants: preparation of an antimicrobial polylactide feedstock material. *J Pharm Sci*. 2015;104(3):1099-1107.
18. Goyanes A, Buanz AB, Hatton GB, Gaisford S, Basit AW. 3D printing of modified-release aminosalicylate (4-ASA and 5-ASA) tablets. *Eur J Pharm Biopharm*. 2015;89:157-162.
19. Skowyra J, Pietrzak K, Alhnan MA. Fabrication of extended-release patient-tailored prednisolone tablets via fused deposition modelling (FDM) 3D printing. *Eur J Pharm Sci*. 2015;68:11-17.
20. Wei C, Solanki NG, Vasoya JM, Shah AV, Serajuddin AT. Development of 3D printed tablets by fused deposition modeling using polyvinyl alcohol as polymeric matrix for rapid drug release. *J Pharm Sci*. 2020;109(4):1558-1572.
21. Ehtezazi T, Algellay M, Islam Y, Roberts M, Dempster NM, Sarker SD. The application of 3D printing in the formulation of multilayered fast dissolving oral films. *J Pharm Sci*. 2018;107(4):1076-1085.
22. Melocchi A, Uboldi M, Parietti F, et al. Lego-inspired capsular devices for the development of personalized dietary supplements: proof of concept with multimodal release of caffeine. *J Pharm Sci*. 2020;109(6):1990-1999.
23. Khaled SA, Burley JC, Alexander MR, Roberts CJ. Desktop 3D printing of controlled release pharmaceutical bilayer tablets. *Int J Pharm*. 2014;461(1-2):105-111.
24. Khaled SA, Burley JC, Alexander MR, Yang J, Roberts CJ. 3D printing of tablets containing multiple drugs with defined release profiles. *Int J Pharm*. 2015;494(2):643-650.
25. Tagami T, Ando M, Nagata N, et al. Fabrication of naftopidil-loaded tablets using a semisolid extrusion-type 3D printer and the characteristics of the printed hydrogel and resulting tablets. *J Pharm Sci*. 2019;108(2):907-913.
26. Cui M, Li Y, Wang S, et al. Exploration and preparation of a dose-flexible regulation system for levetiracetam tablets via novel semi-solid extrusion three-dimensional printing. *J Pharm Sci*. 2019;108(2):977-986.
27. Huang W, Dispoto GJ. Producing Diffusion-Controlled Release Devices. *[Patent]*. 2018.
28. Huang W, Dispoto GJ. Producing Ingredient Delivery Devices for Release Control. *[Patent]*. 2018.
29. Huang W, Dispoto GJ. Producing Erosion-Controlled Release Devices. *[Patent]*. 2018.
30. Edgar J, Tint S. Additive manufacturing technologies: 3D printing, rapid prototyping, and direct digital manufacturing. *Johnson Matthey Tech Rev*. 2015;59(3):193-198.
31. Lipson H, Kurman M. *Fabricated: The New World of 3D Printing*. John Wiley & Sons; 2013.
32. Gibson I, Rosen D, Stucker B. Binder jetting. In: *Additive Manufacturing Technologies*. Springer; 2015:205-218.
33. Alhnan MA, Okwuosa TC, Sadia M, Wan K-W, Ahmed W, Arafat B. Emergence of 3D printed dosage forms: opportunities and challenges. *Pharm Res*. 2016;33(8):1817-1832.
34. Fina F, Madla CM, Goyanes A, Zhang J, Gaisford S, Basit AW. Fabricating 3D printed orally disintegrating printlets using selective laser sintering. *Int J Pharm*. 2018;541(1-2):101-107.
35. Wu BM, Borland SW, Giordano RA, Cima LG, Sachs EM, Cima MJ. Solid free-form fabrication of drug delivery devices. *J Control Release*. 1996;40(1-2):77-87.
36. Aulton ME, Taylor KM. *Aulton's Pharmaceutics: The Design and Manufacture of Medicines*. Elsevier Health Sciences; 2017.
37. Katstra W, Palazzolo R, Rowe C, Giritlioglu B, Teung P, Cima M. Oral dosage forms fabricated by three dimensional Printing™. *J Control Release*. 2000;66(1):1-9.
38. Zema L, Melocchi A, Maroni A, Gazzaniga A. Three-dimensional printing of medicinal products and the challenge of personalized therapy. *J Pharm Sci*. 2017;106(7):1697-1705.
39. Yu DG, Zhu L-M, Branford-White CJ, Yang XL. Three-dimensional printing in pharmaceutics: promises and problems. *J Pharm Sci*. 2008;97(9):3666-3690.
40. Lewis WEP, Rowe CW, Cima MJ, Materna PA. *System and method for uniaxial compression of an article, such as a three-dimensionally printed dosage form [Patent]*. 2003.
41. Wang C-C, Tejwani MR, Roach WJ, et al. Development of near zero-order release dosage forms using three-dimensional printing (3-DP™) technology. *Drug Dev Ind Pharm*. 2006;32(3):367-376.
42. Yu DG, Shen XX, Branford-White C, Zhu LM, White K, Yang XL. Novel oral fast-disintegrating drug delivery devices with predefined inner structure fabricated by Three-Dimensional Printing. *J Pharm Pharmacol*. 2009;61(3):323-329.
43. Lee K-J, Kang A, Delfino JJ, et al. Evaluation of critical formulation factors in the development of a rapidly dispersing captopril oral dosage form. *Drug Dev Ind Pharm*. 2003;29(9):967-979.
44. Rowe C, Katstra W, Palazzolo R, Giritlioglu B, Teung P, Cima M. Multimechanism oral dosage forms fabricated by three dimensional printing™. *J Control Release*. 2000;66(1):11-17.
45. Infanger S, Haemmerli A, Iliev S, Baier A, Stoyanov E, Quodbach J. Powder bed 3D-printing of highly loaded drug delivery devices with hydroxypropyl cellulose as solid binder. *Int J Pharm*. 2019;555:198-206.
46. Antic A, Gibson I, Hapgood K. Exploring the 3D printing binder jetting process for pharmaceutical applications. *Chemeca*. 2018;2018:256.
47. Lee A, Sudau K, Ahn KH, Lee SJ, Willenbacher N. Optimization of experimental parameters to suppress nozzle clogging in inkjet printing. *Ind Eng Chem Res*. 2012;51(40):13195-13204.

48. Guo Y, Patanwala HS, Bognet B, Ma AW. Inkjet and inkjet-based 3D printing: connecting fluid properties and printing performance. *Rapid Prototyp J*. 2017;23(3):562-576.
49. Derby B. Inkjet printing of functional and structural materials: fluid property requirements, feature stability, and resolution. *Annu Rev Mater Res*. 2010;40:395-414.
50. Mishra I, Liu P, Shetty A, Hrenya CM. On the use of a powder rheometer to probe defluidization of cohesive particles. *Chem Eng Sci*. 2020;214:115422.
51. Schulze D. *Powders and Bulk Solids: Behavior, Characterization, Storage and Flow. 2008*. Springer; 2003.
52. Ganesan V, Rosentrater KA, Muthukumarappan K. Flowability and handling characteristics of bulk solids and powders—a review with implications for DDGS. *Biosyst Eng*. 2008;101(4):425-435.
53. Abdullah EC, Geldart D. The use of bulk density measurements as flowability indicators. *Powder Technol*. 1999;102(2):151-165.
54. Gibbs JW. *The Collected Works of J. Willard Gibbs*. New York: Longmans, Green; 1928:2 (v).
55. Hutchings IM, Martin GD. *Inkjet Technology for Digital Fabrication*. John Wiley & Sons; 2012.
56. Lenz E, Löbmann K, Rades T, Knop K, Kleinebudde P. Hot melt extrusion and spray drying of co-amorphous indomethacin-arginine with polymers. *J Pharm Sci*. 2017;106(1):302-312.
57. Vromans H, Bolhuis GK, Lerk CF, van de Biggelaar H, Bosch H. Studies on tableting properties of lactose. VII. The effect of variations in primary particle size and percentage of amorphous lactose in spray dried lactose products. *Int J Pharm*. 1987;35(1):29-37.
58. Sebhatu T, Alderborn G. Relationships between the effective interparticulate contact area and the tensile strength of tablets of amorphous and crystalline lactose of varying particle size. *Eur J Pharm Sci*. 1999;8(4):235-242.
59. Ashby M. *Materials Selection in Mechanical Design*. New York: Elsevier; 2005.
60. Kaialy W, Martin GP, Ticehurst MD, et al. Characterisation and deposition studies of recrystallised lactose from binary mixtures of ethanol/butanol for improved drug delivery from dry powder inhalers. *AAPS J*. 2011;13(1):30-43.
61. Sinka IC, Cunningham JC, Zavaliangos A. Analysis of tablet compaction. II. Finite element analysis of density distributions in convex tablets. *J Pharm Sci*. 2004;93(8):2040-2053.
62. Al-Sabbagh M, Polak P, Roberts R, Reynolds G, Sinka I. Methodology to estimate the break force of pharmaceutical tablets with curved faces under diametrical compression. *Int J Pharm*. 2019;554:399-419.
63. Pitt KG, Heasley MG. Determination of the tensile strength of elongated tablets. *Powder Technol*. 2013;238:169-175.